Basic Nanostructure of Stratum Corneum Lipid Matrices Based on Ceramides [EOS] and [AP]: A Neutron Diffraction Study

Annett Schröter,[†*] Doreen Kessner,[†] Mikhail A. Kiselev,[‡] Thomas Hauß,[§¶] Silva Dante,[§] and Reinhard H. H. Neubert[†]

[†]Martin Luther Universität Halle-Wittenberg, Institute of Pharmacy, Halle (Saale), Germany; [‡]Frank Laboratory of Neutron Physics, Joint Institute for Nuclear Research, Dubna, Moscow Region, Russia; [§]Helmholtz Centre Berlin for Materials and Energy, Berlin, Germany; and [¶]Technische Universität Darmstadt, Department of Chemistry, Physical Biochemistry, Darmstadt, Germany

ABSTRACT The goal of this study was to investigate the nanostructure of SC lipid model membranes comprising the most relevant SC lipids such as the unique-structured ω-acylceramide [EOS] in a near natural ratio with neutron diffraction. In models proposed recently the presence of ceramide [EOS] and FFA are necessary for the formation of one of the two existent crystalline lamellar phases of the SC lipids, the long-periodicity phase as well as for the normal barrier function of the SC. The focus of this study was placed on the influence of the FFA BA on the membrane structure and its localization within the membrane based on the ceramides [EOS] and [AP]. The internal nanostructure of such membranes was obtained by Fourier synthesis from the experimental diffraction patterns. The resulting neutron scattering length density profiles showed that the exceptionally long ceramide [EOS] is arranged in a short-periodicity phase created by ceramide [AP] by spanning through the whole bilayer and extending even further into the adjacent bilayer. Specifically deuterated BA allowed us to determine the exact position of this FFA inside this SC lipid model membrane. Furthermore, hydration experiments showed that the presented SC mimic system shows an extremely small intermembrane hydration of ~1 Å, consequently the headgroups of the neighboring leaflets are positioned close to each other.

INTRODUCTION

The SC represents the outermost layer of the mammalian skin and serves as the main skin barrier (1). The superficial layer consists of dead cells, the corneocytes, filled with the protein keratin. The corneocytes are further embedded in a matrix of multilamellar organized lipid membranes (2). Several transport studies showed that the lipid matrix is the major diffusion-rate limiting pathway, as most of the drugs applied topically pass the SC through the multilamellar organized lipids (3,4). The knowledge and comprehension of the nanostructure and the relative properties of the SC on the molecular level, in particular of the SC lipids is essential for the understanding of drug penetration through the SC as well as for the development of new dermal drug delivery systems.

The absence of phospholipids as a main component of biological membranes is one important feature that characterizes the unique lipid composition as well as the unique properties of the SC. The major lipid classes that can be extracted from the SC are CER, CHOL, and FFA (5–7). It is generally known that the main constituent, the ceramides, play a key role in the structuring and maintenance of the barrier function of the skin (8,9).

To date, a detailed picture of the molecular organization of the lipids in the SC has not been fully elucidated. To characterize the SC lipid matrix and to understand its properties, two approaches arise: one is based on native SC lipids isolated from, e.g., human skin (10–17), the other concept is based on well-defined synthetic SC lipids (18–21). Several x-ray diffraction studies showed (18,20) that a SC lipid model system based on synthetic substances with a defined structure would be the most favorable one, due to the fact that the impact of each lipid species to the nanostructure of SC lipid matrix can be studied. The application of neutron diffraction offers new possibilities to investigate the nanostructure of SC lipid systems as first shown in the work of Kiselev et al. (21) on a quaternary SC lipid model matrix. The advantages of the application of neutron diffraction for the study of SC lipid systems and the properties of those lipid membranes revealed by neutron diffraction experiments were reviewed in Kessner et al. (22). Furthermore, neutron diffraction on oriented multilamellar lipid membranes extended the experimental pool in SC lipid studies due to the two principal advantages of neutron over x-ray scattering. First, there is the possibility of the determination of the sign of the structure factors by contrast variation, which is necessary for the further evaluation of the neutron SLD profiles $\rho_s(x)$. The neutron SLD profiles give information about the nanostructure of the lipid membrane. The contrast variation was achieved by partial exchange of water by

Submitted September 18, 2008, and accepted for publication May 28, 2009.

*Correspondence: annett.ruettinger@pharmazie.uni-halle.de

Abbreviations used: SC, stratum corneum; a.u., arbitrary units; BA, behenic acid; CA, cerotic acid; CER, ceramide; CER[EOS], 30-linoyloxy-triacontanoic acid-[(2S,3R)-1,3-dihydroxyocta-dec-4-en-zyl]-amide; CER[AP], *N*-(α-hydroxyoctadecanoyl)-phytosphingosine; CHOL, cholesterol; FFA, free fatty acid; FWHM, full width at half maximum; LPP, long-periodicity phase; PA, palmitic acid; RH, relative humidities; SF, structure factors; SLD, scattering length density; SPP, short-periodicity phase; TA, tetracosanoic acid.

Editor: Huey W. Huang.

0006-3495/09/08/1104/11 $2.00

doi: 10.1016/j.bpj.2009.05.041

heavy water. Second, the exchange of hydrogen by deuterium atoms in the lipid molecules enables the exact determination of the labeled position within the lipid membrane as the scattering length of hydrogen and deuterium atoms differs significantly. The calculation of specific membrane parameters from the SLD profile, such as the region of the polar headgroups and thickness of the intermembrane space, further improves and intensifies the knowledge about such SC lipid model matrices as shown by Kiselev et al. (21).

The main constituent of the SC, the ceramides (23,24) are known to play a key role in structuring and maintaining the SC barrier function. However, the function of each of the nine subclasses of ceramides has not been elucidated until now. To estimate their individual role, the experimental methods that are applied commonly to characterize the physical properties are x-ray diffraction, vibrational spectroscopy such as Fourier transform infrared and Fourier transform Raman spectroscopy, as well as differential scanning calorimetry as reviewed in Wartewig and Neubert (25). Until now, the focus was placed primarily on the influence of the hydrocarbon chain length and in particular, the predominant role of CER[EOS] was especially discussed as its unique structure was closely attributed to the existence of a LPP of 130 Å in the SC lipid matrix (26). Different experimental methods showed that the SC lipids are organized in two crystalline lamellar phases, the mentioned LPP and the so-called SPP with a lamellar spacing of ~60 Å (27–32). To the contrary, we observed a different structural organization of the SC lipids by studying the influence of different ceramide classes on the membrane assembly in neutron diffraction experiments. Particularly the polarity of the headgroups exceeds the influence of the hydrocarbon chain, especially the influence of the length of the hydrocarbon chain. The short-chain phytosphingosine CER[AP] with a high polarity founded on four OH-groups, induces the formation of a superstable membrane with a short periodicity of ~45 Å, the so called armature reinforcement model (33). Investigations on a ternary system composed of CER[EOS]/CER[AP]/CHOL (33:22:45%, w/w) indicated only the presence of a short-periodicity phase of 45 Å due to the strong influence of CER[AP] on the membrane assembling process. The long-chain ω-acylceramide CER[EOS] is forced by CER[AP] to arrange inside this short phase, extending the long alkyl chain residue into the adjacent membrane layer. The calculated SLD profile underlines this assumption. As a major result, the absence of the LPP was observed despite the presence of CER[EOS] (34). This has to be emphasized, because this result marks a shift of paradigm about the influence of ceramides on the nanostructure of such SC lipid model systems (35). Furthermore, we concluded from other experiments that focused on the influence of the chain-length of FFA on the nanostructure of SC lipid model membranes based on CER[AP] (36), that the long-chain FFA need to interdigitate into the membrane size dictated by CER[AP]. It was shown that CER[AP] creates a superstable structure, which is not disturbed by the alteration of the FFA chain-length.

The ultimate aim is to design a lipid mixture that mimics the lipid organization of human SC to a high extent and can therefore be used as a substitute for the native SC to study the efficacy of penetration enhancer as well as retarder molecules on a molecular level. The intention of this study was to investigate SC lipid model membranes based on CER[EOS]/CER[AP]/CHOL/FFA, therefore containing the most relevant lipids in a near natural ratio. The corresponding SLD profile was used to describe the internal membrane nanostructure. Further, the influence of single defined lipid species on the membrane assembling process is discussed. Concerning the location of some lipid classes inside the lipid matrix, the use of specific deuterated molecules is addressed. Finally, the influence of hydration on the structure of the SC lipid model membrane is shown to substantiate the creation of a superstable structure by CER[AP].

MATERIALS AND METHODS

Materials

The ceramides CER[AP] and CER[EOS] were generously provided by Evonik Goldschmidt GmbH (Essen, Germany). To increase the chemical purity of CER[EOS] >96%, the substance was treated using the middle pressure liquid chromatographic technique on a silica gel column with a chloroform/methanol gradient. CER[AP] had a purity >96% and was used as received. The identity of both ceramides indicated by the parameter of molecular mass (CER[EOS] = 1012 g/mol; CER[AP] = 600 g/mol) was proven by mass spectrometry. CHOL, PA, docosanoic (BA), TA, and CA were purchased from Sigma-Aldrich (Taufkirchen, Germany), and the deuterated fatty acid species, docosanoic-7,7,8,8-d_4-acid (further referred as d_7BA, 99.2 atom % D) and docosanoic-22,22,22-d_3-acid (d_{22}BA, 99.2 atom % D) were purchased from Dr. Ehrenstorfer GmbH (Augsburg, Germany) and used as received. Quartz slides (Spectrosil 2000) were received from Saint-Gobain (Wiesbaden, Germany).

Sample preparation

Four compositions of SC lipid model systems were studied as detailed in Table 1, whereby only the FFA component was changed.

The appropriate mixture of lipids was dissolved in a chloroform/methanol mixture (1:1 V/V) with a total lipid concentration of 10 mg/mL. A volume of 1200 μL of the lipid solution was spread over a 6.4 cm × 2.5 cm quartz surface and was first dried at room temperature and afterward under vacuum. After the removal of the organic solvent a subsequent heating (>60°C) and cooling cycle was applied, whereby the sample was kept in horizontal position and at 100% relative humidity to decrease the mosaicity of the sample.

The benefit of the annealing procedure for the a model membrane based on CER[AP] is shown in Fig. 1, whereby the rocking curve of the model membrane before the annealing procedure was carried out is presented in Fig. 1 *A*, whereas Fig. 1 *B* displays the rocking curve of the same sample

TABLE 1 Composition of the SC lipid model membranes

Composition	Ratio % (w/w)
CER[EOS]/CER[AP]/CHOL/palmitic acid	23:10:33:33
CER[EOS]/CER[AP]/CHOL/BA	23:10:33:33
CER[EOS]/CER[AP]/CHOL/TA	23:10:33:33
CER[EOS]/CER[AP]/CHOL/CA	23:10:33:33

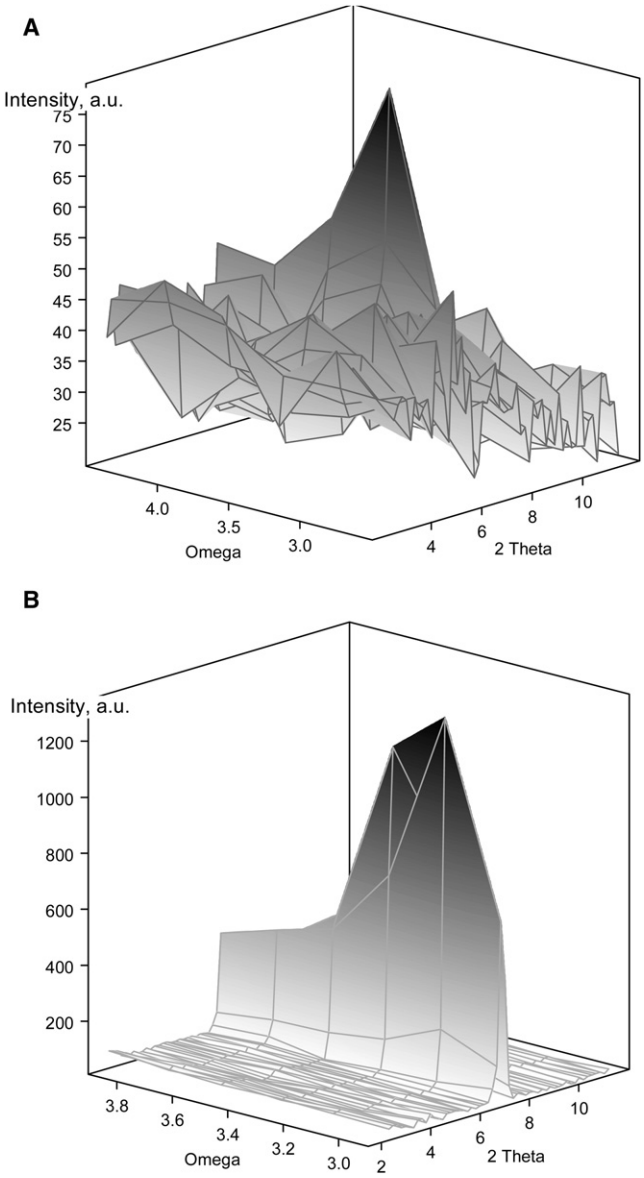

FIGURE 1 Rocking curve around a fixed angle 2θ to verify the mosaicity of the sample composed of ceramide[AP]/cholesterol/stearic-d_{35}-acid /cholesterol sulfate. The intensity scale is normalized to the intensity of the primary beam (50,000 Monitor counts/step). (*A*) Example for a sample with high mosaicity and low intensity before the annealing procedure was carried out. (*B*) Illustration of the same sample after heating at 75°C and cooling at 100% RH.

after the heating and cooling cycle was carried out. Limited neutron beam time does not allow a systematic monitoring of all samples under investigation. This annealing procedure was necessary to obtain a better orientation of the membranes and increase the size of the liquid crystal domains. The averaged thickness of the lipid film on the quartz slide was 7.5 μm. Such an oriented multilamellar stack of lipids on a quartz slide (preparation according to the procedure of Seul and Sammon (37)) is used commonly in neutron diffraction experiments (38–40).

Neutron diffraction experiment

The neutron diffraction patterns from each sample were collected at the V1 diffractometer of the Berlin Neutron Scattering Centre of the Helmholtz Centre Berlin for Materials and Energy, Berlin, Germany, located at a cold neutron source, with a wavelength of $\lambda = 5.23$ Å and a sample-to-detector distance of 102.38 cm. The neutron diffraction in the reflection setup was used to collect the data of the one-dimension diffraction experiment. The detailed experimental setup is described elsewhere (36). The diffraction intensities were recorded either as $\theta - 2\theta$ -scan (high mosaicity samples), or as rocking scan (ω-scan), whereby the sample was rocked around the expected Bragg position θ, by $\theta \pm 2°$. Both ways allowed the collection of up to five orders of diffraction. The two-dimensional position sensitive ^{3}He detector (20 cm × 20 cm area, 1.5 mm × 1.5 mm spatial resolution) was used.

All samples were measured in thermostated aluminum cans at a fixed temperature of 32°C and RH of either 57% or 98% RH. The humidity was controlled using an aqueous saturated sodium bromide solution for 57% RH and a saturated solution of potassium sulfate for 98% RH. This procedure is described in detail elsewhere (41). To vary the difference of the scattering length density between the lipid membrane and the water layer (neutron contrast), the atmosphere in the sample chamber was adjusted to up to four different H_2O/D_2O molar compositions (92:8, 80:20, 50:50, and 0:100). An equilibration time of 12 h was allowed after each change of aqueous solution.

In the neutron diffraction patterns, the scattering intensity I (a.u.) was measured as a function of the scattering vector Q (in reciprocal Å). The latter is defined as $Q = (4\pi \sin\theta)/\lambda$, in which 2θ is the scattering angle and λ is the wavelength of the neutron beam. From the positions of a series of equidistant peaks (Q_n), the lamellar repeat unit d, or d-spacing, of a lamellar phase was calculated using the equation $Q_n = 2n\pi/d$, whereby n stands for the order number of the diffraction peak. The integrated intensities were calculated using Gaussian fits to the Bragg reflections received in the neutron diffraction experiment. From the integrated peak intensity the absolute value of the SF was calculated as $|F_H| = A_h(\theta) \times \sqrt{h \times I_h}$ (h is the diffraction order) with Lorentz correction h and absorption factor $A_h(\theta)$, whereby the absorption factors were calculated according to Eq. 1 (42):

$$A_h(\theta) = \left[\frac{\sin\theta}{2\mu L} \times \left(1 - \exp\left(-\frac{2\mu L}{\sin\theta}\right)\right)\right]^{-\frac{1}{2}}, \qquad (1)$$

where θ is the Bragg angle, μ is the linear absorption coefficient that was calculated for $\lambda = 5.23$ Å to $\mu = 6.1$ cm^{-1} (21), and the thickness L of the lipid film amounts to $L = 7.5$ μm. Table 2 shows exemplarily the absorption factors and SF for the sample CER[EOS]/CER[AP]/CHOL/BA (23:10:33:33) at 8% D_2O and 57% RH.

The structure of the bilayer was conventionally analyzed by the construction of the neutron SLD profiles $\rho_s(x)$ (a.u.) across the bilayer as Fourier synthesis as shown in Eq. 2 (43):

$$\rho_s(x) = \frac{2}{d}\sum_{h=1}^{h_{max}} F_h \times \cos\left(\frac{2 \times \pi \times h \times x}{d}\right), \qquad (2)$$

where F_h is the SF of the diffraction peak of the order h, and d is the lamellar repeat distance calculated from the peak position as describe above. For symmetrical and hydrated bilayers it was shown that the phase problem of the SF simplifies to the determination of the symbol "+" or "−" for each SF (42). This can be accomplished by the variation of the H_2O/D_2O ratio (contrast variation) (39). An example of the dependency of the

TABLE 2 Absorption factors and structure factors along with the uncertainties from the counting statistics for the sample composed of CER[EOS]/CER[AP]/CHOL/BA (23:10:33:33) at 8% D_2O and 57% RH

Diffraction order h	Absorption factor	Structure factor ± error
1	1.043	6.656 ± 0.054
2	1.021	3.764 ± 0.077
3	1.014	4.692 ± 0.085
4	1.011	2.227 ± 0.106
5	1.007	2.825 ± 0.138

membrane structure factor F_h of the order $h = 1, 2, 3, 4$, and 5 on the D_2O content in water vapor is presented in Fig. 2. The procedure for the evaluation of the neutron diffraction data is described in detail elsewhere (38,39,42,43).

All presented SLD profiles are displayed in a relative scale instead of an absolute scale. The reason for this presentation is the large error that would result in using the absolute scaling method. The determination of the absolute scale (or more precisely the relative absolute scale as defined by Wiener and White (39)) relies on the knowledge of the number of water molecules per lipid. With this information we can place the difference density of e.g., profile measurements at 8% D_2O and 50% D_2O on an absolute scale. In the case of the investigated SC model membranes the intermembrane space was determined to ~0.1 nm (21). With a headgroup area of 0.3 nm^2 (between pure CER (0.25 nm^2) and cholesterol (0.37 nm^2)) the space for one water molecule can be calculated with a volume of 0.03 nm^3. But this estimation suffers from many obstacles such as the error to the intermembrane space of 30%, ranging from 0.7 nm to 1.3 nm, not well-defined area per lipid ranging from 0.4 nm^2 to 0.2 nm^2 (an estimation from Dahlen and Pascher (44)), and it is not well justified, if we can use the water volume of 0.03 nm^3 or a smaller one more close to the van der Vaals volume of 0.0146 nm^3). Alternatively, it is possible to determine the water content gravimetrically. But with the low water content of ceramide-based membranes the difference in weight between a dry and a hydrated sample is very small. All together, the calculation of the absolute scale provides results with an exceedingly large error, which will render it useless.

The localization of a specific deuterium label within the lipid membrane is reflected by the positive difference in the SLD between samples containing either deuterated or protonated FFA. According to Eq. 3 the difference was calculated for each structure factor:

$$\Delta F_h^{\mathrm{Deut}} = F_h(deut) - F_h(prot). \quad (3)$$

The difference SLD can be calculated by using Eq. 2 and by substituting F_h with $\Delta F_h^{\mathrm{Deut}}$ (45–47).

RESULTS AND DISCUSSION

Finding an appropriate SC lipid matrix model

In this approach the ternary system CER[EOS]/CER[AP]/CHOL (33:22:45%, w/w) was completed by a FFA. The FFA found in the SC are generally of the saturated non-branched variety and are the third major lipid fraction of the SC next to the ceramides and cholesterol. Therefore, a lipid system composed of all three main constituents resembles the native SC lipid matrix to a high extent and can give more precise information concerning its properties. Furthermore, it is stated in the literature, that the presence of FFA is necessary for the formation of the LPP (48) as well as for the normal barrier function of the SC (49).

The first approach was to add the rather short-chain FFA PA to the ternary SC lipid matrix because its chain-length is in the range of the short-chain ceramide [AP]. The diffraction patterns of the model system containing the ceramides [EOS] and [AP] together with CHOL and PA showed reflections resulting from phase-separated CHOL-crystals and phase-separated PA (Fig. 3). The characterization of the internal membrane nanostructure could not be carried out due to the strong phase separation (three different phases). Only the lamellar repeat distance with $d = 42.2$ Å could be evaluated. In the further approach, the FFA palmitic acid was substituted by the longer-chained BA (22:0), TA (C24:0), and CA (C26:0), respectively. In the native SC the fraction of FFA mainly contains FFA with chain length in the region between C24 and C26 (50,51). Therefore, the use of long-chained FFA in such SC model systems will resemble more closely the natural SC lipid matrix. For the mixture of CER[EOS]/CER[AP]/CHOL/BA, diffraction patterns were received as demonstrated in Fig. 4. These patterns exhibit a one-phase multilamellar membrane with only a small fraction of cholesterol crystals. The presence of small amounts of crystalline CHOL does not influence

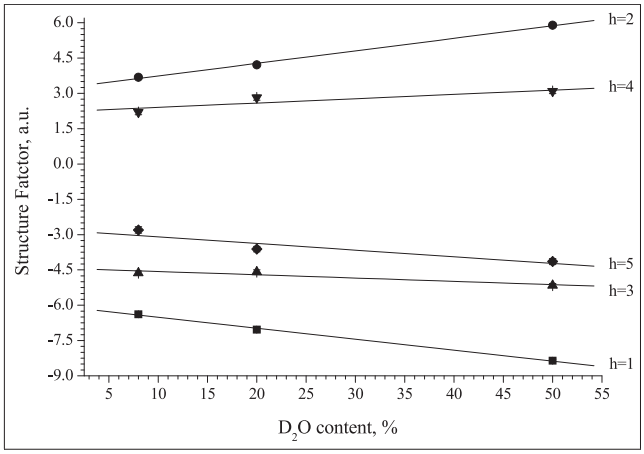

FIGURE 2 Example of the dependency of the membrane structure factor F_h of the order $h = 1, 2, 3, 4$, and 5 on the D_2O content in water vapor. The linearity of the structure factors versus the D_2O content is shown for the sample composed of CER[EOS]/CER[AP]/CHOL/BA (23:10:33:33% w/w) at 32°C and 57% RH.

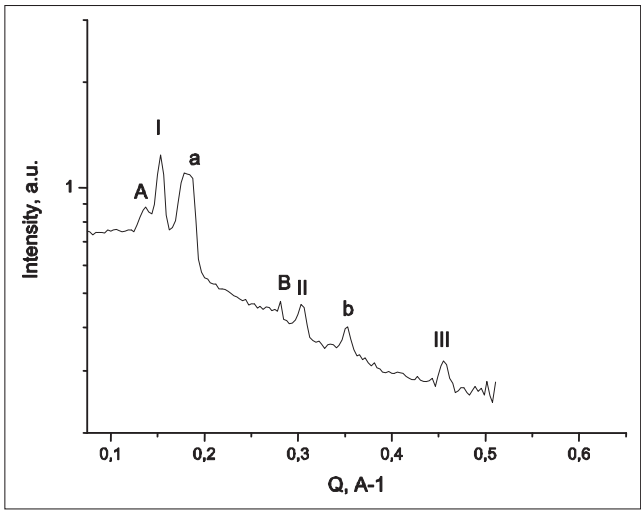

FIGURE 3 Neutron diffraction pattern for the CER[EOS]/CER[AP]/CHOL/PA membrane with the composition of 23:10:33:33% (w/w) at 57% humidity, an H_2O/D_2O ratio of 50:50 and 32°C. The roman numbers indicate the first, second, and third order diffraction peaks for the model membrane, small letters indicate the [010] and [020] diffraction peaks from pure CHOL crystals, and capital letters indicate the diffraction of a palmitic acid rich phase.

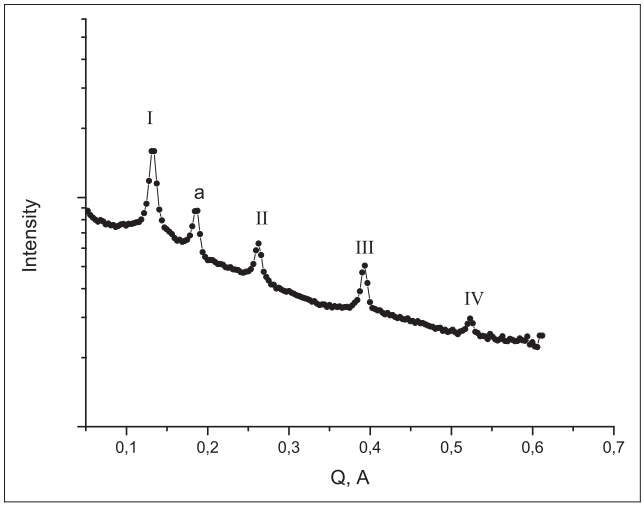

FIGURE 4 Neutron diffraction pattern for the CER[EOS]/CER[AP]/CHOL/BA membrane with the composition of 23:10:33:33% (w/w) at 57% humidity, an H_2O/D_2O ratio of 50:50 and $T = 32°C$. The roman numbers indicate the first, second, third, and fourth order diffraction peaks for the model membrane and small letter indicates the [010] diffraction peak from pure CHOL crystals.

the multilamellar lipid organization as described in other studies (18,52–54).

A system composed of a long-chain and a short-chain ceramide combined with a long-chain FFA as it is typical for the SC lipid matrix causes a reasonable miscibility of the lipids and a good solubility of cholesterol inside the model matrix. Interestingly, the amount of CER[AP] in this SC model system could be reduced on addition of BA to the ternary system (34). To characterize the internal membrane nanostructure, the neutron SLD profile SLD $\rho_s(x)$ was calculated as described in Materials and Methods.

Discussion of the membrane profile $\rho_s(x)$

From the neutron diffraction pattern of the SC model membrane comprised of CER[EOS]/CER[AP]/CHOL/BA, each diffraction peak was fitted by a Gaussian function after background subtraction. This was carried out with the program PeakFit (SYSTAT Software, San Jose, CA). The center of the Gaussian function was used to characterize the peak position and to calculate the membrane repeat distance d, which amounts to $d = 48.3$ Å $\pm$ 0.1 Å. Additionally, phase-separated cholesterol crystals were present in the model membrane that can be deduced from the [010] reflection located at $Q = 0.18$ Å^{-1}, representing diffraction from the triclinic crystal with the lattice parameters $a = 14.172$ Å, $b = 34.209$ Å, $c = 10.481$ Å, and $\alpha = 96.64°$, $\beta = 90.67°$, $\gamma = 96.32°$ (55). Despite the presence of the long-chain ceramide CER[EOS], the long-periodicity phase, the LPP was not detected. In fact, a periodicity of ~48 Å indicated the presence of a bilayer in the range of two opposing CER[AP] molecules as discussed previously (34,35).

In a recent study (21), we investigated the quaternary SC lipid model system CER[AP]/CHOL/PA/ChS (55:25:15:5% w/w) that will therefore be assigned as the reference system. The comparability of the lamellar repeat distances, the d-values of the reference system ($d = 45.6$ Å) and of the present system ($d = 48.3$ Å) allows the parallel presentation of both SLD profiles in a.u. as shown in Fig. 5 The details of this normalization procedure are described elsewhere (36). In accordance to the observations for the ternary system based on the ceramides [EOS] and [AP] together with CHOL the major results taken from the comparison of the SLD profiles of quaternary SC lipid model membrane containing CER[EOS], CER[AP], CHOL, and BA with the reference membrane (CER[AP]/CHOL/PA/ChS) include:

i. The smaller SLD at the position of the polar headgroup region of the CER[EOS]/CER[AP]/CHOL/BA membrane in comparison to reference matrix is caused by the CH_2 groups of the CER[EOS] molecules that protrude into the adjacent layer to fit into the membrane size created by CER[AP]. The negative SLD of the CH_2 groups (-3.0×10^9 cm^{-2}) at the polar headgroup region leads to a reduction in the SLD of the polar headgroup region, whereas in the reference system the CH_2 groups are not present in this area and cannot produce such a reduction of the SLD.
ii. The minimum in the center of the bilayer representing the CH_3 groups is less pronounced than in the reference system. This is an evidence, that also in the center of the membrane CH_2 groups are present. Therefore, it can be stated again that the long hydrocarbon chains of the CER[EOS] molecules protrude through the bilayer, which leads to an increase of the SLD because the CH_2 groups show a higher SLD compared to the CH_3 groups.

Taking both experimental results into account, it can be concluded that the arrangement of CER[EOS] inside the lipid matrix is similar to the already described ternary system

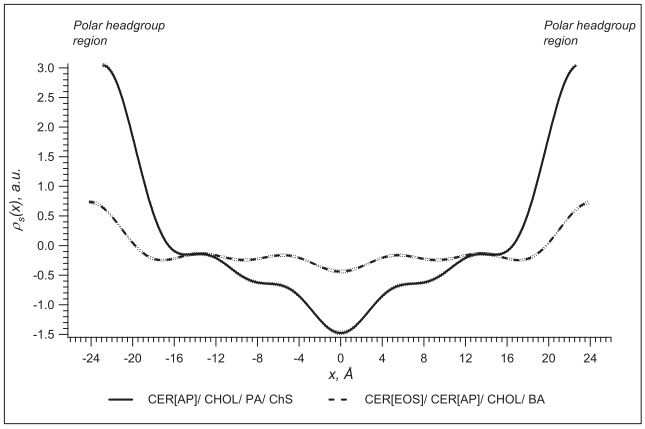

FIGURE 5 Neutron SLD profile $\rho_s(x)$ across the CER[EOS]/CER[AP]/CHOL/BA membrane (23:10:33:33% w/w) at 57% humidity, and an H_2O/D_2O ratio of 92:8 and $T = 32°C$. The CER[AP]/CHOL/PA/ChS (55:25:15:5% w/w) membrane was measured under the same conditions.

(34): CER[EOS] is positioned inside a phase with a short-periodicity by spanning a bilayer and extending into adjacent layer. In contrast to the ternary system, the presented SC lipid model matrix was completed by the inclusion of the long-chain FFA BA. Furthermore, due to this FFA addition the amount of CER[AP] could be reduced from 22% to 10% (w/w), which is close to the fraction of CER[AP] found in human SC (4–7%) (9,56). To estimate the exact position of BA inside this SC lipid model membrane partially deuterated BA was applied.

Identification of the exact position of BA inside the lipid matrix

It was found that in SC lipid model membranes based on CER[AP] and also containing a long-chain FFA, the FFA protrudes through the adjacent layer to fit into the superstable membrane matrix created by CER[AP] (36). The application of specifically deuterated FFA supplied the direct experimental evidence of the interdigitation of the FFA (57). To identify the exact position of the FFA in SC lipid model membranes based on the ceramides [EOS] and [AP], two membranes have been investigated, each containing partially deuterated BA. The exact composition is listed in Table 3. The calculated SLD profiles of the samples containing specifically deuterated BA showed distinct differences when compared to the sample containing the protonated FFA. In Fig. 6 the comparison of the SLD profiles of the membrane containing either protonated BA (CER[EOS]/CER[AP]/CHOL/BA, EOS_BA) or deuterated BA (CER[EOS]/CER[AP]/CHOL/d_{22}-BA, EOS-d_{22}BA) with the deuteration at the terminal methyl group is illustrated. The SLD profile of the deuterated SC model matrix shows a distinct maximum in the center of the membrane (CH_3-group region), which is related to a high SLD of the terminal CD_3-groups of BA. To further identify the exact position of the label within the membrane, the difference SLD profile $\Delta\rho_s^{Deut}(x)$ was calculated according to Eq. 3 and then fitted by a Gaussian function seen in Fig. 7. The result of this fit is presented in Table 4. For this broad maximum with a fixed center at $x_0 = 0$ Å, the FWHM parameter equals ~6 Å (region from −3 to 3 Å). The latter comprises the membrane region in which the terminal alkyl groups interdigitate and therefore, a high density of deuterium atoms appears. The maxima

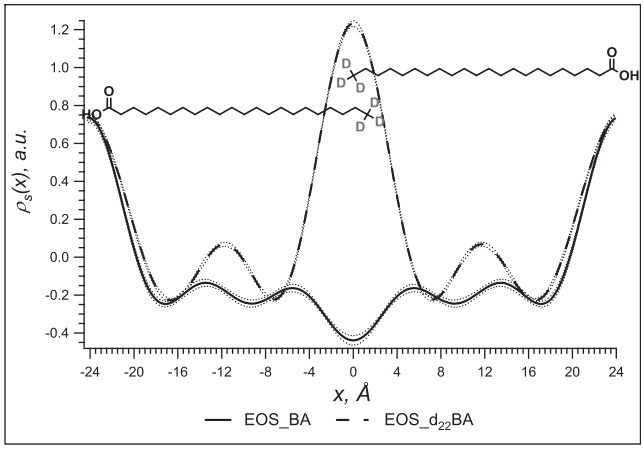

FIGURE 6 Comparison of the neutron SLD profiles of a membrane composed of CER[EOS]/CER[AP]/CHOL/and either protonated BA (EOS_BA, *solid line*) or deuterated d_{22}-BA (EOS-d_{22}BA, *dashed line*) at $T = 32°C$, 57% RH, and 8% D_2O. Dotted lines: corresponding errors. To visualize the proposed arrangement the molecular structure of d_{22}BA BA was introduced.

at the edges of the profile are attributed to the polar headgroup region (21). The high scattering length at ~−15 and 15 Å corresponds to the position of cholesterol (58).

The same procedure was applied to the sample containing BA specifically deuterated in the methylene group region (CER[EOS]/CER[AP]/CHOL/d_7-BA; EOS_d_7BA). The comparison of the SLD profiles of the protonated and deuterated sample as well as the difference SLD $\Delta\rho_s^{Deut}(x)$ of both are presented in (Fig. 8 and (Fig. 9, respectively. Next to the two maxima belonging to the polar headgroups, the membrane profile of CER[EOS]_d_7BA showed two additional maxima that were assigned to the labeled CD_2-groups with a high density of deuterium atoms and with positive coherent SLD (see (Fig. 8). Both positions have been fitted by a Gaussian function and the center of both Gaussian function was determined at $x_{C_7D_2,C_8D_2} = 16.10$ Å and −16.10 Å, respectively (see also Table 4).

To visualize this result, the following model was applied: a bilayer, formed by two opposing BA-molecules reveals a repeat distance d of ~55 Å, estimated by the values of 1.5 Å for a CH_3-group and 1.25 Å for one CH_2-group (59). When this hypothetical BA-bilayer is compared to the SC lipid model system that exhibits a d-value of ~48 Å, a difference

TABLE 3 Composition of the model SC lipid system

CER[EOS]/CER[AP]/CHOL/d_7-BA: (23:10:33:33% w/w)	EOS_d_7BA
CER[EOS]/CER[AP]/CHOL/d_{22}-BA: (23:10:33:33% w/w)	EOS-d_{22}BA

Only the deuterated FFA component was varied.

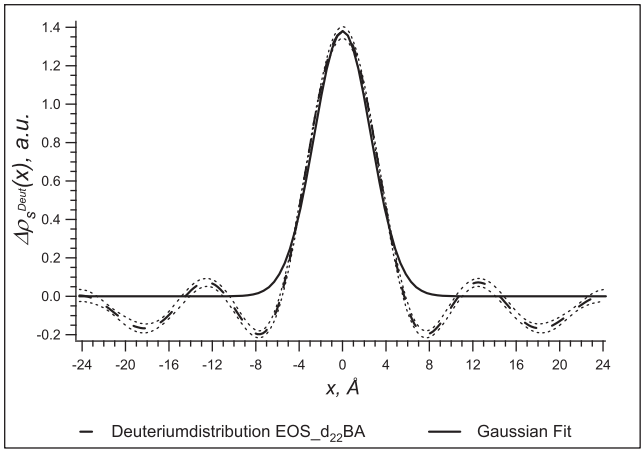

FIGURE 7 Difference SLD profile for CER[EOS]/CER[AP]/CHOL/d_{22}-BA membrane (*dashed line*). Dotted lines: corresponding errors to the difference SLD profile. Fat solid line: fit of the difference SLD by a Gaussian function (= deuterium distribution).

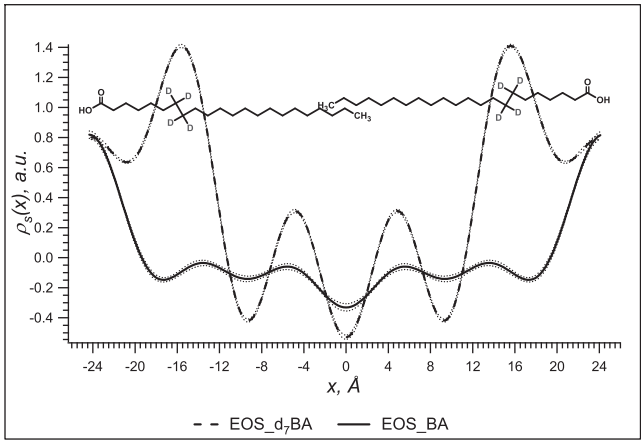

FIGURE 8 Comparison of the SLD profiles of a membrane composed of CER[EOS]/CER[AP]/CHOL/and either protonated BA (EOS_BA, *solid line*) or deuterated d_7-BA (EOS_d_7BA, *dashed line*) at $T = 32°C$, 57% RH, and 8% D_2O. Dotted lines: corresponding errors. To visualize the proposed arrangement the molecular structure of d_7-BA was introduced.

of ~7 Å occurs. We suppose that this difference between both hypothetical and real membrane is compensated by the interdigitation of the terminal butyl (5.25 Å) or pentyl (6.5 Å) residues of the BA chain in the SC lipid membrane. The relevant maxima of the deuterium distribution $\Delta\rho_s^{\mathrm{Deut}}(x)$ correspond to the region of C_7D_2–C_8D_2 with the center x at 16.10 Å and −16.10 Å, respectively (see Fig. 8). From the FWHM it can be deduced that the CH_2-groups region represents the largest region within such a membrane (21). Therefore, the FWHM (5.67 Å) comprises the region with the highest density of deuterium atoms. This region can be calculated as 16.10 ± 1/2 FWHM (±13.27 Å − ±18.94 Å). In the hypothetical BA bilayer, the position of C_7 and C_8 may be estimated as $x_{C_7H_2-C_8H_2} = +18$ Å and −18 Å, respectively. Related to the fitted position at 16.10 Å, the difference of ~1.9 Å would indicate only an interdigitation of the terminal propyl-residue. Consequently, a shift of the position of C_7D_2–C_8D_2 from 18 Å to 13 Å would be inside these error margins for the case of an interdigitation of terminal butyl residues in the center of the membrane. Due to truncation errors of the applied Fourier synthesis, the center of the membrane profile can not be taken into account.

The evidence of a stretched, gel-like conformation of the BA molecule arises from the condensing effect of cholesterol on acyl chains (60,61). Cholesterol increases the trans conformation of the chains and decreases the tilt angle. In a recent study it is suggested that short-chain ceramides, like cholesterol, may have a similar ordering effect itself (62).

Summarizing, the study of the SC lipid model matrices composed of CER[EOS]/CER[AP]/CHOL/BA and containing the deuterated BA showed the arrangement of the FFA inside the bilayer. The application of specific deuterated BA-derivatives caused different local contrasts and therefore, the labeled molecular regions could be identified inside the membrane profile. For all four membrane constituents, a reasonable localization inside the lipid matrix could be suggested on the basis of the neutron SLD profile.

TABLE 4 Lamellar repeat distance *d* and the position *x* of the deuterated label of the FFA inside one lipid leaflet for each deuterated FFA containing membrane at 32°C, 8% D_2O, and 57% RH

SC lipid model membrane	*d* [Å]	Position *x* of label [Å]
EOS-d_{22}-BA	48.52 ± 0.27	CD_3-group: 0.00 ± 0.09
EOS-d_7-BA	48.28 ± 0.08	CD_2-groups ±: 16.10 ± 0.09

Influence of hydration on the membrane structure

To deepen our knowledge about the SC model systems containing the ceramides [EOS] and [AP] along with CHOL and BA the influence of the hydration on the membrane structure

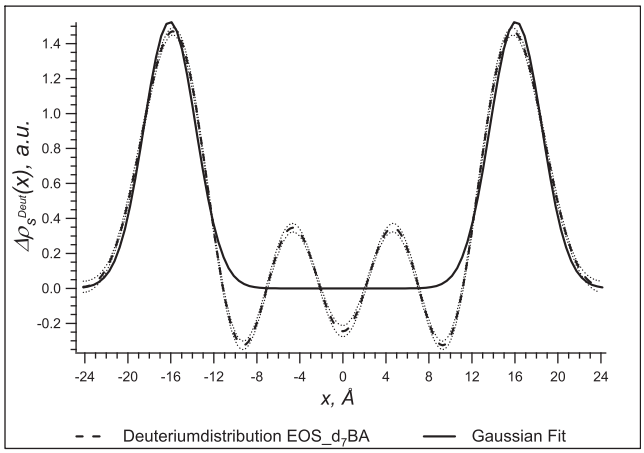

FIGURE 9 Difference SLD profile for CER[EOS]/CER[AP]/CHOL/d_7-BA membrane (*dashed line*). Dotted lines: corresponding errors to the difference SLD profile. Fat solid line: fit of difference SLD by two Gaussian functions (= deuterium distribution).

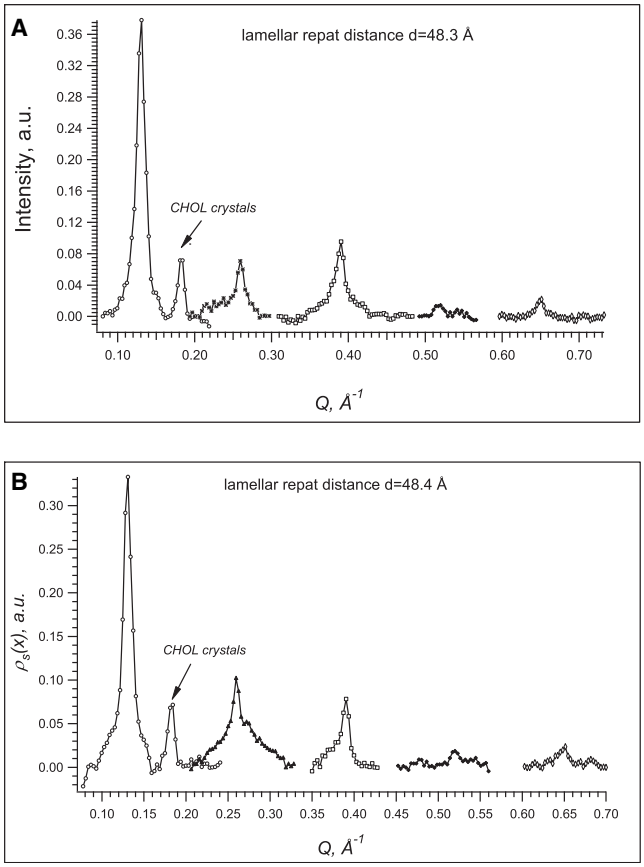

FIGURE 10 Neutron diffraction patterns of the CER[EOS]/CER[AP]/CH/BA membrane at (*A*) 57% RH, and (*B*) 98% RH, respectively. Measurements were done at D_2O/H_2O contrast of 8/92 and $T = 32°C$.

was studied. From literature, it is known, that the SC lipids, in particular the ceramides show only a small tendency to bind water (63).

The model system CER[EOS]/CER[AP]/CHOL/BA (23:10:33:33% w/w) was measured at 57% relative humidity (RH) and 98% RH, respectively. The collected diffraction patterns are presented in Fig. 10, *A* and *B*, respectively. From the peak position the lamellar repeat distances d were calculated and amount to $d = 48.3$ Å at 57% RH and 48.4 Å at 98% RH, respectively. Because of the almost identical values of the periodicities, a minimal influence of the degree of humidity on the hydration behavior of the lipids as well as on the membrane structure was concluded. From the calculated neutron SLD profiles (data not shown), several membrane parameters were determined by applying a fit-procedure as described in the work of Kiselev et al. (21) and are summarized in Table 5. As we pointed out in Ruettinger et al. (36) the dependence of the Fourier profile on the D_2O content in water vapor enables the calculation of the water distribution function ρ_w across the bilayer according to Eq. 4.

TABLE 5 Membrane parameters as taken from the neutron SLD profile

SC system	Molecular group	x_0 [Å]*	σ [Å]	FWHM [Å]†
CER[EOS]-BA 57% RH	Polar headgroups	24.15	2.43 ± 0.03	5.49 ± 0.06
CER[EOS]-BA 98% RH	Polar headgroups	24.20	2.36 ± 0.03	5.78 ± 0.14

*$x_0 = \frac{d}{2}$ is fixed.
†FWHM $= 2\sigma\sqrt{2\ln 2}$.

$$\rho_w = \rho_{50\%D_2O} - \rho_{8\%D_2O} \quad (4)$$

To compare the water distribution across the bilayer at the different relative humidities the water distribution function was calculated for the EOS_BA membrane at 57% RH and at 98% RH, respectively. Fig. 11, *A* and *B*, show the water distribution function across the membrane at 57% RH (Fig. 11 *A*) and at 98% RH (Fig. 11 *B*), respectively. The minima and maxima in the center of the membrane are due to truncation errors.

In principle such lipid membranes as discussed here can be divided into hydrophilic and hydrophobic regions. The

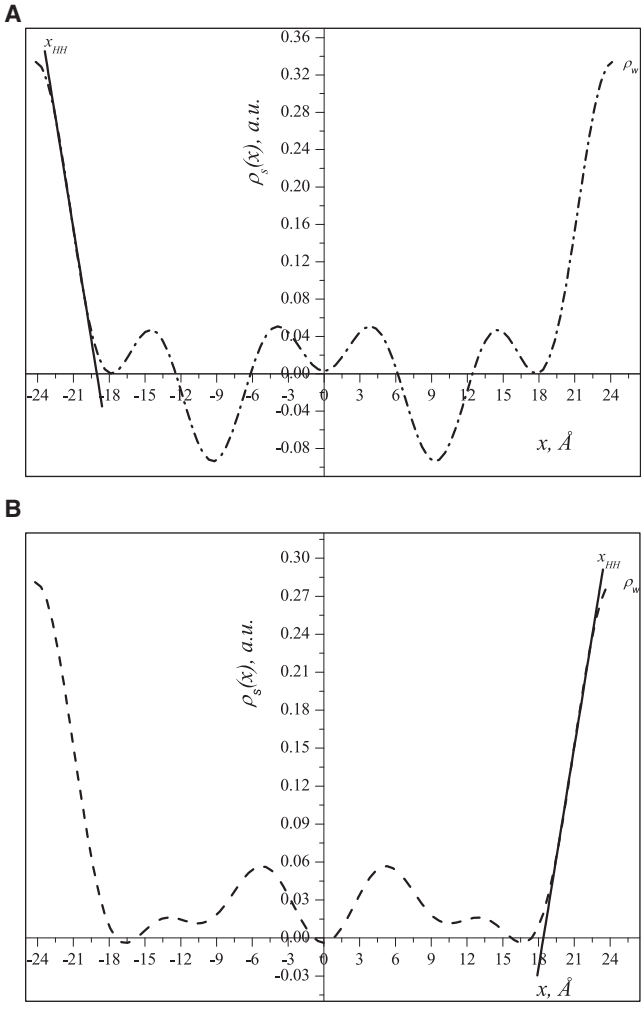

FIGURE 11 Water distribution function $\rho_w(x)$ across the CER[EOS]_BA membrane at (*A*) 57% RH, and (*B*) 98% RH, respectively. The *HH* boundary is determined via linear fit as shown here.

TABLE 6 Structural parameters of the membrane containing BA at 32°C and 8% D_2O at different humidities

EOS_BA, humidity	d [Å]*	x_{PH} [Å]†	x_{HH} [Å]‡	Thickness of hydrophobic layer [Å]	Thickness of hydrophilic layer [Å]
57% RH	48.3 ± 0.1	24.15	19.0 ± 0.5	38.1 ± 0.9	5.1 ± 0.5
98% RH	48.4 ± 0.1	24.20	18.4 ± 0.6	36.8 ± 1.2	5.8 ± 0.6

*d, repeat distance.
†x_{PH}, position of polar headgroups.
‡x_{HH}, hydrophilic-hydrophobic boundary.

boundary between both regions, the hydrophilic-hydrophobic (*HH*) boundary is located at the position x where the water distribution function ρ_w is near to zero. The *HH* boundary determines the thickness of the hydrophilic as well as lipophilic part of the bilayer. The position of the *HH* boundary for the SC lipid model membrane at each humidity as well as the thickness of the hydrophobic and hydrophilic layer are summarized in Table 6. From those results it can be concluded that although the value for the thickness of the hydrophilic layer is slightly higher at 98% RH, there are no significant changes due to the hydration process.

As described by Kiselev et al. (21), SC lipid model membranes based on CER[AP] do not show a region of intermembrane space at 57% RH. From the neutron SLD profile, it can be derived that the present model matrix, EOS_BA, and the reference system share an extremely small intermembrane hydration of ~1 Å. This value was received as difference between the d-spacings at 57% RH and at water excess in the work of Kiselev et al. (21). Consequently, the headgroups of the neighboring leaflets are positioned close to each other. The distance between the two adjacent maxima of the headgroups d_{PH} is equal to the membrane repeat distance d_m. Therefore, the position of the polar headgroups x_{PH} is determined by $d_m/2$ whereby the x_{PH}-value increases with increasing hydration. From that fact it can be deduced, that the hydration of the polar headgroups increases. This theory is drawn on the increasing value of the FWHM, indicating an enhancement of the area per headgroup at 98% RH. The low intermembrane space does not allow the calculation of the thickness of the water layer d_W as $d_W = d - d_m$ as the space resolution according to $0.6 \times d/h_m$ (h_m = number of diffraction orders) was calculated to 5.8 Å (21). In this study, a difference of 0.1 Å was observed between the periodicities of the membrane measured at 57% RH and at 98% RH, respectively. This distinction could be inside certain error margins, indicating that no significant influence of hydration on the membrane assembling process occurs. On the other hand, based on the membrane parameters taken from the SLD profiles $\rho_s(x)$, a slight increase of the hydration of the headgroups at higher humidity may be supposed.

SUMMARY

Summarizing, it can be stated that the SC lipid model system composed of CER[EOS]/CER[AP]/CHOL/BA (23:10:33:33% w/w) represents a reasonable model of the native lipid matrix. The composition comprises the three major lipid classes in an appropriate ratio. Inside the ceramide fraction, the model contains the CER[EOS] that is attributed to be crucial for the proper skin barrier function (12,64). Behenic acid represents the most abundant subtype of the skin's FFA (1). The presented quaternary system forms multilamellar oriented bilayers and supplies reasonable good diffraction patterns in the neutron experiments. By analyzing the neutron SLD profiles resulting from this study, the arrangement of all lipid components inside the lipid matrix could be concluded as visualized in Fig. 12.

Numerous former studies proclaimed the coexistence of two lamellar phases in the SC, namely the SPP of ~60 Å and LPP of ~130 Å (15,16,26). The latter is particularly associated with the presence of CER[EOS] that therefore is regarded to be a prerequisite for proper barrier functions. The existence of the LPP including its organization and the inducing or preventing conditions for its formation are currently a matter of debate, comprising of many pros and cons (65,66). From x-ray diffraction patterns of CER[EOS] as bulk substance at hydrated state, the formation of a phase with a periodicity of ~130 Å could be proven (D. Kessner and G. Brezesinski, unpublished data). In mixtures with other prominent SC lipids in particular with CER[AP], a multilamellar membrane based on CER[EOS] only exhibits the formation of a short-periodicity phase. From former studies it is known that this characteristic phase is induced

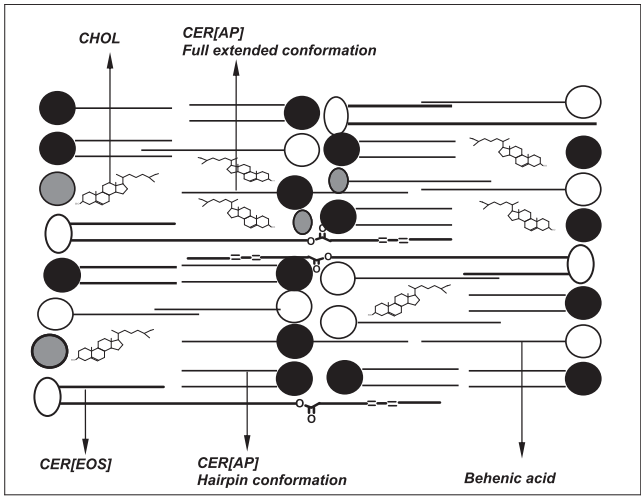

FIGURE 12 Schematic presentation of the CER[EOS]/CER[AP]/CHOL/BA (23:10:33:33% w/w) model matrix.

predominantly by the short-chain CER[AP], which is characterized by a distinct headgroup polarity (34). In the work of Kessner et al. (34,35), it was stated that the influence of the headgroup polarity exceeds the influence of the chain length in terms of the membrane assembling. This experimental fact could also be proven in this study. Further, this study contributed what we believe are insights to the discussions on the crucial importance of the SPP for the skin barrier.

The authors thank Evonik Goldschmidt GmbH (Essen, Germany) for the donation of CER [AP] and CER[EOS].

The work was supported by the German Research Foundation (DFG) (NE 427/17-1), the ''Graduiertenförderung des Landes Sachsen-Anhalt'', and the Helmholtz Centre Berlin for Materials and Energy (Berlin, Germany).

REFERENCES

1. Wertz, P. W., and B. van den Bergh. 1998. The physical, chemical and functional properties of lipids in the skin and other biological barriers. *Chem. Phys. Lipids.* 91:85–96.
2. Elias, P. M. 1983. Epidermal lipids, barrier function, and desquamation. *J. Invest. Dermatol.* 80 (Suppl.):44s–49s.
3. Bodde, H. E., I. Vandenbrink, H. K. Koerten, and F. H. N. Dehaan. 1991. Visualization of in vitro percutaneous penetration of mercuric-chloride—transport through intercellular space versus cellular uptake through desmosomes. *J. Control. Release.* 15:227–236.
4. Talreja, P., N. K. Kleene, W. L. Pickens, T. F. Wang, and G. B. Kasting. 2001. Visualization of the lipid barrier and measurement of lipid path-length in human stratum corneum. *AAPS PharmSci.* 3:E13.
5. Gray, G., and H. Yardley. 1975. Different populations of pig epidermal cells: isolation and lipid composition. *J. Lipid Res.* 16:441–447.
6. Gray, G. M., and R. J. White. 1978. Glycosphingolipids and ceramides in human and pig epidermis. *J. Invest. Dermatol.* 70:336–341.
7. Yardley, H. J., and R. Summerly. 1981. Lipid composition and metabolism in normal and diseased epidermis. *Pharmacol. Ther.* 13:357–383.
8. Holleran, W. M., M. Q. Man, W. N. Gao, G. K. Menon, P. M. Elias, et al. 1991. Sphingolipids are required for mammalian epidermal barrier function. Inhibition of sphingolipid synthesis delays barrier recovery after acute perturbation. *J. Clin. Invest.* 88:1338–1345.
9. Coderch, L., O. Lopez, A. de la Maza, and J. L. Parra. 2003. Ceramides and skin function. *Am. J. Clin. Dermatol.* 4:107–129.
10. Bouwstra, J. A., G. S. Gooris, K. Cheng, A. Weerheim, W. Bras, et al. 1996. Phase behavior of isolated skin lipids. *J. Lipid Res.* 37:999–1011.
11. Bouwstra, J. A., G. S. Gooris, F. E. Dubbelaar, A. M. Weerheim, A. P. Ijzerman, et al. 1998. Role of ceramide 1 in the molecular organization of the stratum corneum lipids. *J. Lipid Res.* 39:186–196.
12. Bouwstra, J. A., F. E. Dubbelaar, G. S. Gooris, A. M. Weerheim, and M. Ponec. 1999. The role of ceramide composition in the lipid organisation of the skin barrier. *Biochim. Biophys. Acta.* 1419:127–136.
13. Bouwstra, J. A., G. S. Gooris, F. E. Dubbelaar, and M. Ponec. 2001. Phase behavior of lipid mixtures based on human ceramides: coexistence of crystalline and liquid phases. *J. Lipid Res.* 42:1759–1770.
14. White, S. H., D. Mirejovsky, and G. I. King. 1988. Structure of lamellar lipid domains and corneocyte envelopes of murine stratum corneum. An x-ray diffraction study. *Biochemistry.* 27:3725–3732.
15. McIntosh, T. J., M. E. Stewart, and D. T. Downing. 1996. X-ray diffraction analysis of isolated skin lipids: reconstitution of intercellular lipid domains. *Biochemistry.* 35:3649–3653.
16. McIntosh, T. J. 2003. Organization of skin stratum corneum extracellular lamellae: diffraction evidence for asymmetric distribution of cholesterol. *Biophys. J.* 85:1675–1681.
17. Ongpipattanakul, B., M. L. Francoeur, and R. O. Potts. 1994. Polymorphism in stratum corneum lipids. *Biochim. Biophys. Acta.* 1190: 115–122.
18. de Jager, M. W., G. S. Gooris, M. Ponec, and J. A. Bouwstra. 2005. Lipid mixtures prepared with well-defined synthetic ceramides closely mimic the unique stratum corneum lipid phase behavior. *J. Lipid Res.* 46:2649–2656.
19. de Jager, M. W., G. S. Gooris, I. P. Dolbnya, W. Bras, M. Ponec, et al. 2004. Novel lipid mixtures based on synthetic ceramides reproduce the unique stratum corneum lipid organization. *J. Lipid Res.* 45:923–932.
20. de Jager, M. W., G. S. Gooris, I. P. Dolbnya, M. Ponec, and J. A. Bouwstra. 2004. Modelling the stratum corneum lipid organisation with synthetic lipid mixtures: the importance of synthetic ceramide composition. *Biochim. Biophys. Acta.* 1664:132–140.
21. Kiselev, M. A., N. Y. Ryabova, A. M. Balagurov, S. Dante, T. Hauss, et al. 2005. New insights into the structure and hydration of a stratum corneum lipid model membrane by neutron diffraction. *Eur. Biophys. J.* 34:1030–1040.
22. Kessner, D., A. Ruettinger, M. A. Kiselev, S. Wartewig, and R. H. Neubert. 2008. Properties of ceramides and their impact on the stratum corneum structure. Part 2: stratum corneum lipid model systems. *Skin Pharmacol. Physiol.* 21:58–74.
23. Raith, K., H. Farwanah, S. Wartewig, and R. H. H. Neubert. 2004. Progress in the analysis of stratum corneum ceramides. *Eur. J. Lipid Sci. Technol.* 106:561–571.
24. Ponec, M., A. Weerheim, P. Lankhorst, and P. Wertz. 2003. New acylceramide in native and reconstructed epidermis. *J. Invest. Dermatol.* 120:581–588.
25. Wartewig, S., and R. H. H. Neubert. 2007. Properties of ceramides and their impact on the stratum corneum structure: a review. *Skin Pharmacol. Physiol.* 20:220–229.
26. Bouwstra, J. A., F. E. Dubbelaar, G. S. Gooris, and M. Ponec. 2000. The lipid organisation in the skin barrier. *Acta Derm. Venereol. Suppl. (Stockh.).* 208:23–30.
27. Laugel, C., N. Yagoubi, and A. Baillet. 2005. ATR-FTIR spectroscopy: a chemometric approach for studying the lipid organisation of the stratum corneum. *Chem. Phys. Lipids.* 135:55–68.
28. Curdy, C., A. Naik, Y. N. Kalia, I. Alberti, and R. H. Guy. 2004. Non-invasive assessment of the effect of formulation excipients on stratum corneum barrier function in vivo. *Int. J. Pharm.* 271:251–256.
29. Bouwstra, J. A., G. S. Gooris, J. A. van der Spek, and W. Bras. 1991. Structural investigations of human stratum corneum by small-angle x-ray scattering. *J. Invest. Dermatol.* 97:1005–1012.
30. Bouwstra, J. A., G. S. Gooris, W. Bras, and D. T. Downing. 1995. Lipid organization in pig stratum corneum. *J. Lipid Res.* 36:685–695.
31. Pilgram, G. S., A. M. Engelsma-van Pelt, J. A. Bouwstra, and H. K. Koerten. 1999. Electron diffraction provides new information on human stratum corneum lipid organization studied in relation to depth and temperature. *J. Invest. Dermatol.* 113:403–409.
32. Pilgram, G. S., D. C. Vissers, H. van der Meulen, S. Pavel, S. P. Lavrijsen, et al. 2001. Aberrant lipid organization in stratum corneum of patients with atopic dermatitis and lamellar ichthyosis. *J. Invest. Dermatol.* 117:710–717.
33. Kiselev, M. 2007. Conformation of ceramide 6 molecules and chain-flip transitions in the lipid matrix of the outermost layer of mammalian skin, the stratum corneum. *Crystallogr. Rep.* 52:525–528.
34. Kessner, D., M. Kiselev, S. Dante, T. Hauss, P. Lersch, et al. 2008. Arrangement of ceramide [EOS] in a stratum corneum lipid model matrix: new aspects revealed by neutron diffraction studies. *Eur. Biophys. J.* 37:989–999.
35. Reference deleted in proof.
36. Ruettinger, A., M. A. Kiselev, T. Hauss, S. Dante, A. M. Balagurov, et al. 2008. Fatty acid interdigitation in stratum corneum model membranes: a neutron diffraction study. *Eur. Biophys. J.* 37:759–771.

37. Seul, M., and M. J. Sammon. 1990. Preparation of surfactant multilayer films on solid substrates by deposition from organic solution. *Thin Solid Films*. 185:287–305.

38. Worcester, D. L., and N. P. Franks. 1976. Structural analysis of hydrated egg lecithin and cholesterol bilayers. II. Neutron diffraction. *J. Mol. Biol.* 100:359–378.

39. Wiener, M. C., and S. H. White. 1991. Fluid bilayer structure determination by the combined use of x-ray and neutron-diffraction. 1. Fluid bilayer models and the limits of resolution. *Biophys. J.* 59:162–173.

40. Katsaras, J., D. S. Yang, and R. M. Epand. 1992. Fatty-acid chain tilt angles and directions in dipalmitoyl phosphatidylcholine bilayers. *Biophys. J.* 63:1170–1175.

41. Hauss, T., S. Dante, N. A. Dencher, and T. H. Haines. 2002. Squalane is in the midplane of the lipid bilayer: implications for its function as a proton permeability barrier. *Biochim. Biophys. Acta.* 1556:149–154.

42. Franks, N. P., and W. R. Lieb. 1979. The structure of lipid bilayers and the effects of general anesthetics. An x-ray and neutron diffraction study. *J. Mol. Biol.* 133:469–500.

43. Nagle, J. F., and S. Tristram-Nagle. 2000. Structure of lipid bilayers. *Biochim. Biophys. Acta.* 1469:159–195.

44. Dahlen, B., and I. Pascher. 1979. Molecular arrangements in sphingolipids—thermotropic phase-behavior of tetracosanoylphytosphingosine. *Chem. Phys. Lipids.* 24:119–133.

45. Buldt, G., H. U. Gally, A. Seelig, J. Seelig, and G. Zaccai. 1978. Neutron diffraction studies on selectively deuterated phospholipid bilayers. *Nature.* 271:182–184.

46. Hauss, T., G. Buldt, M. P. Heyn, and N. A. Dencher. 1994. Light-induced isomerization causes an increase in the chromophore tilt in the M intermediate of bacteriorhodopsin: a neutron diffraction study. *Proc. Natl. Acad. Sci. USA.* 91:11854–11858.

47. Dante, S., T. Hauss, and N. A. Dencher. 2003. Insertion of externally administered amyloid beta peptide 25–35 and perturbation of lipid bilayers. *Biochemistry.* 42:13667–13672.

48. de Jager, M. W., G. S. Gooris, I. P. Dolbnya, W. Bras, M. Ponec, et al. 2003. The phase behavior of skin lipid mixtures based on synthetic ceramides. *Chem. Phys. Lipids.* 124:123–134.

49. Mao-Qiang, M., P. M. Elias, and K. R. Feingold. 1993. Fatty acids are required for epidermal permeability barrier function. *J. Clin. Invest.* 92:791–798.

50. Bonte, F., A. Saunois, P. Pinguet, and A. Meybeck. 1997. Existence of a lipid gradient in the upper stratum corneum and its possible biological significance. *Arch. Dermatol. Res.* 289:78–82.

51. Norlen, L., I. Nicander, A. Lundsjo, T. Cronholm, and B. Forslind. 1998. A new HPLC-based method for the quantitative analysis of inner stratum corneum lipids with special reference to the free fatty acid fraction. *Arch. Dermatol. Res.* 290:508–516.

52. Huang, J., J. T. Buboltz, and G. W. Feigenson. 1999. Maximum solubility of cholesterol in phosphatidylcholine and phosphatidylethanolamine bilayers. *Biochim. Biophys. Acta.* 1417:89–100.

53. Ali, M. R., K. H. Cheng, and J. Huang. 2006. Ceramide drives cholesterol out of the ordered lipid bilayer phase into the crystal phase in 1-palmitoyl-2-oleoyl-sn-glycero-3-phosphocholine/cholesterol/ceramide ternary mixtures. *Biochemistry.* 45:12629–12638.

54. Brzustowicz, M. R., V. Cherezov, M. Caffrey, W. Stillwell, and S. R. Wassall. 2002. Molecular organization of cholesterol in polyunsaturated membranes: microdomain formation. *Biophys. J.* 82:285–298.

55. Shieh, H. S., L. G. Hoard, and C. E. Nordman. 1977. Crystal structure of anhydrous cholesterol. *Nature.* 267:287–289.

56. Farwanah, H., R. Neubert, S. Zellmer, and K. Raith. 2002. Improved procedure for the separation of major stratum corneum lipids by means of automated multiple development thin-layer chromatography. *J. Chromatogr. B Analyt. Technol. Biomed. Life Sci.* 780:443–450.

57. Reference deleted in proof.

58. Kessner, D., M. A. Kiselev, T. Hauss, S. Dante, S. Wartewig, et al. 2008. Localization of partially deuterated cholesterol in quaternary SC lipid model membranes: a neutron diffraction study. *Eur. Biophys. J.* 37:1051–1057.

59. Fox, M. A., and J. K. Whitesell. 1995. Organic chemistry — Fundamentals, mechanisms, bioorganic applications. Spektrum Akademischer Verlag, Heidelberg, Germany.

60. Czub, J., and M. Baginski. 2006. Comparative molecular dynamics study of lipid membranes containing cholesterol and ergosterol. *Biophys. J.* 90:2368–2382.

61. McIntosh, T. J. 1978. The effect of cholesterol on the structure of phosphatidylcholine bilayers. *Biochim. Biophys. Acta.* 513:43–58.

62. Carrer, D. C., S. Schreier, M. Patrito, and B. Maggio. 2006. Effects of a short-chain ceramide on bilayer domain formation, thickness, and chain mobility: DMPC and asymmetric ceramide mixtures. *Biophys. J.* 90:2394–2403.

63. Raudenkolb, S., S. Wartewig, G. Brezesinski, S. S. Funari, and R. H. Neubert. 2005. Hydration properties of N-(alpha-hydroxyacyl)-sphingosine: x-ray powder diffraction and FT-Raman spectroscopic studies. *Chem. Phys. Lipids.* 136:13–22.

64. Bouwstra, J. A., G. S. Gooris, F. E. Dubbelaar, and M. Ponec. 2002. Phase behavior of stratum corneum lipid mixtures based on human ceramides: the role of natural and synthetic ceramide 1. *J. Invest. Dermatol.* 118:606–617.

65. Pfeiffer, S., G. Vielhaber, J. P. Vietzke, K. P. Wittern, U. Hintze, et al. 2000. High-pressure freezing provides new information on human epidermis: simultaneous protein antigen and lamellar lipid structure preservation. Study on human epidermis by cryoimmobilization. *J. Invest. Dermatol.* 114:1030–1038.

66. Al-Amoudi, A., J. Dubochet, and L. Norlen. 2005. Nanostructure of the epidermal extracellular space as observed by cryo-electron microscopy of vitreous sections of human skin. *J. Invest. Dermatol.* 124:764–777.